

Supporting Information

Bioinspired NiFe-Gallate Metal–Organic Frameworks for Highly Efficient Oxygen Evolution Electrocatalysis

Min Fang,^{‡, †} Xutao Gao,^{‡, §} Jing Liang,^{‡, †} Biao Guo,[†] Lie Zou,[†] Jun Lu,[†] Yan Gao,[†] Edmund C. M. Tse^{*, §, #} and Jinxuan Liu^{*, †}

[†] State Key Laboratory of Fine Chemicals, Dalian University of Technology, 116024 Dalian, China.

[§] Department of Chemistry, HKU-CAS Joint Laboratory on New Materials, University of Hong Kong, Hong Kong SAR, China.

[#] HKU Zhejiang Institute of Research and Innovation, 311305 Hangzhou, China.

[‡] These authors contributed equally to this work.

* **Jinxuan Liu** - State Key Laboratory of Fine Chemicals, Dalian University of Technology, 116024 Dalian, China.

E-mail: jinxuan.liu@dlut.edu.cn

* **Edmund C. M. Tse** - Department of Chemistry, HKU-CAS Joint Laboratory on New Materials, University of Hong Kong, Hong Kong SAR, China.

Email: ecmtse@hku.hk

Experimental Details

Chemicals and Materials

Potassium hydroxide (KOH, 95%), nickel chloride hexahydrate ($\text{NiCl}_2 \cdot 6\text{H}_2\text{O}$, 99.9%), and gallic acid monohydrate (GA, 98%) were purchased from Aladdin. Iron (II) chloride tetrahydrate ($\text{FeCl}_2 \cdot 4\text{H}_2\text{O}$, 99.95%) was purchased from Macklin. A customized laboratory water purification system was used to purify deionized (DI) water ($18.2 \text{ } \Omega\text{M}\cdot\text{cm}$ at $25 \text{ } ^\circ\text{C}$). All the above reagents and chemicals were used without further purification in all experiments.

Synthesis of Ni-GA, Fe-GA, and NiFe-GA

The catalysts were prepared by a one-step hydrothermal method. A piece of carbon paper (CP) (area: $2 \times 2 \text{ cm}^2$; thickness: 0.28 mm) was soaked sequentially in 1 M HCl, acetone, DI water, and absolute ethanol for 30 minutes under ultrasonic conditions. Then, the CP was kept in a vacuum drying oven at $60 \text{ } ^\circ\text{C}$ for 8 h. Ni-GA, Fe-GA, and NiFe-GA were synthesized using a previously reported method with slight modifications.^{1,2} Typically, gallic acid monohydrate (H_4gal , 4 mmol) was dissolved in a KOH aqueous solution (5 mL, 0.16 M), and nickel chloride hexahydrate ($\text{NiCl}_2 \cdot 6\text{H}_2\text{O}$, x mmol, x=2, 1.75 and 0) and iron (II) chloride tetrahydrate ($\text{FeCl}_2 \cdot 4\text{H}_2\text{O}$, y mmol, y=0, 0.25, and 2) were dissolved in a KOH aqueous solution (2.5 mL, 0.16 M), respectively. After ultrasonic treatment for 30 min, the mixture was transferred into a 15 mL stainless steel autoclave lined with Teflon. The CP (area: $2 \times 2 \text{ cm}^2$; thickness: 0.28 mm) was vertically placed into the autoclave. Then, the autoclave was sealed and kept at $120 \text{ } ^\circ\text{C}$ for 24 h. After that, the autoclave was naturally cooled down to room temperature. The CP was taken out from the autoclave carefully and rinsed with deionized water and ethanol to remove weakly adsorbed catalysts and

impurities. Finally, the obtained samples were kept at 60 °C under vacuum for 12 h.

Materials Characterization

X-ray diffractometer (XRD, Rigaku Rotaflex, Japan) with CuK α radiation ($\lambda = 1.5418$ nm, 40 kV, 40 mA) was used to record crystallographic information of the catalyst. FTIR spectrometer (Bruker VERTEX 80v) with a narrow band mercury cadmium telluride (MCT) detector was used to obtain important information on the functional groups on the catalyst. Field emission scanning electron microscope (SEM, FEI Nova Nano SEM 450) and transmission electron microscope (TEM, FEI TF30) were used to identify the morphology and map the elemental distribution across the surface of the catalyst. X-ray photon energy spectroscopy (XPS, Thermo VG ESCALAB250) was used to determine the redox state of the sample surface. Raman spectra were recorded using LabRam HR spectrometer (Horiba Jobin Yvon) with a 50X objective microscope. The excitation line was 638 nm with a power of 2.4 mW.

Electrocatalytic Test

All electrochemical tests were performed on an electrochemical workstation (CHI760E, Shanghai, China) at room temperature in a traditional three-electrode system using a Pt wire ($\Phi = 1$ mm) as the counter electrode, the as-prepared catalysts and blank CP (effective geometric area: 1×1 cm²) as the working electrode, and a Hg/HgO electrode as the reference electrode. 1 M KOH was used as the electrolyte for all electrochemical tests.

Cyclic Voltammetry (CV) Measurements

CV experiments were performed in the range of 0.9 - 1.9 V vs. RHE at a scan rate of 50 mV s⁻¹. The working electrodes used for all CV experiments in this work were CP, Ni-GA-CP, Fe-GA-CP, and NiFe-GA-CP, respectively.

Linear Sweep Voltammetry (LSV) Measurements

LSV measurement setting conditions were similar to CV test with 90% iR compensation. High-potential to low-potential reverse scan method with a lower scan rate (5 mV·s⁻¹) was used to obtain an accurate curve without the interference of oxidation peaks.

Electrochemical Active Surface Area (ECSA) Measurements

CVs at different scan rates from 20 to 120 mV·s⁻¹ in the potential range of 0.8 - 0.9 V (vs. RHE) were performed to evaluate the electrochemical active surface area (ECSA) of the as-prepared electrocatalysts. By obtaining capacitive currents ($J_{\text{anodic}} - J_{\text{cathodic}}$) at 0.85 V (vs. RHE), the double-layer capacitance (C_{dl}) is equal to half of the slope.

Stability Tests

Chronopotentiometry (CP) was used to evaluate the stability of the electrocatalysts at 50 mA·cm⁻² and 100 mA·cm⁻² (without iR correction). All the potentials versus Hg/HgO were converted to the reversible hydrogen electrode (RHE) by the Nernst equation ($E_{\text{RHE}} = E_{\text{Hg/HgO}} + 0.098 + 0.059\text{pH}$), and the overpotential of OER was calculated by the equation: $\eta = E_{\text{RHE}} - 1.23$ and Tafel slopes were calculated with the equation: $\eta = b \log j + a$ where η represents the overpotential, b represents the Tafel slope, j represents the current density, and a is the constant.

Computational Methods

The initial Ni-GA and Fe-GA structures were taken from previous literature.³ The NiFe-GA structure was constructed by expanding the Ni-GA structure twice and replacing one Ni atom with a Fe atom. Spin-polarized density functional theory (DFT) calculations were performed to optimize the cell shape and the atomic positions of the structure by Vienna *ab initio* simulation package (VASP)⁴ using the projector augmented wave (PAW) potentials with a planewave cutoff energy of 450 eV.^{5,6} The generalized gradient approximation (GGA) functional of Perdew, Burke, and Ernzerhof (PBE) was applied as the exchange-correlation functional⁷ with Grimme's semiempirical DFT-D3 dispersion correction to describe the van der Waals (vdW) interactions.⁸ To better describe the localized d-electrons of Fe and Ni in GA-MOF structures, the DFT+U approach was utilized with $U_{\text{Fe}} = 5.3$ and $U_{\text{Ni}} = 6.45$, respectively.⁹ The convergence criteria of electronic energies and atomic forces for all calculations were 10^{-5} eV and 0.03 eV/Å. For NiFe-GA calculations, Brillouin-zone integrations were performed with a $4 \times 4 \times 4$ Gamma k-point mesh grid for the bulk structure. To study surface reactions, the most exposed (100) plane was constructed for the adsorption of intermediates, which is consistent with XRD results. A vacuum region of 15 Å was added to the surface to eliminate the effects between two adjacent layers. The (100) plane of Fe-GA, Ni-GA, and NiFe-GA were geometry-optimized by DFT calculation to obtain a stable surface structure. Subsequently, the *O, *OH, and *OOH adsorbed intermediates were optimized by DFT calculation to obtain the energy of each structure. For surface property calculations, half of the bottom layers were fixed at their bulk positions using a $3 \times 3 \times 1$ Gamma k-point grid. The ZPE and

entropy corrections were performed through frequency calculations.

OER overpotential was evaluated by the Nørskov's model¹⁰ with the following steps:



where * represents an adsorption active site on the surface of the catalyst, while *OH, *O, and *OOH denote oxygen intermediates. For each step i , the Gibbs free energy ΔG_i can be calculated using:

$$\Delta G_i = \Delta E + \Delta ZPE - T\Delta S + Ue + \Delta G_{pH} \quad (5)$$

where ΔE is the reaction energy difference between the reactants and the products, ΔZPE is the zero-point energy, ΔS is the entropy change, T represents the finite temperature, e is the charge transferred, U is the applied potential, and ΔG_{pH} is considered as the correction free energy of H^+ .

The overpotential η is computed as:

$$\eta = \max\{\Delta G_1, \Delta G_2, \Delta G_3, \Delta G_4\}/e - 1.23eV \quad (6)$$

Figures and Tables

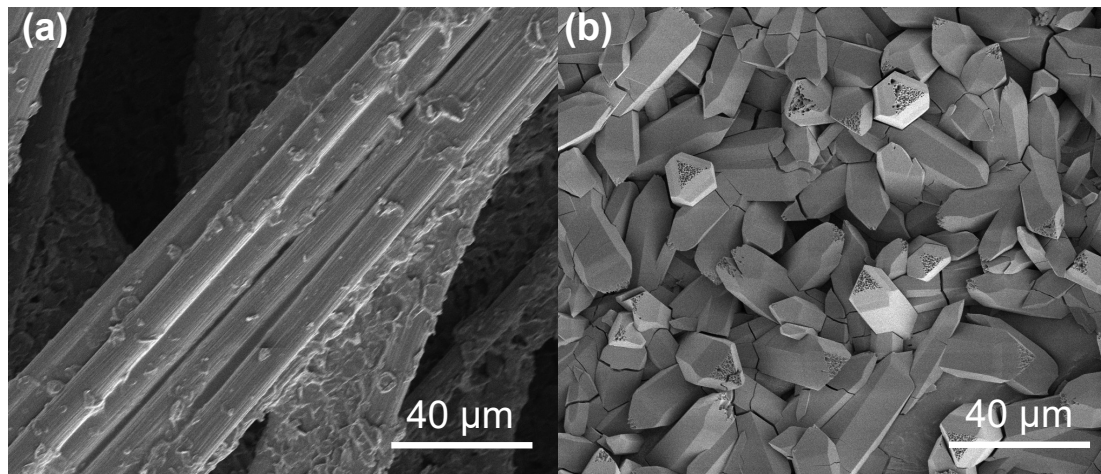


Figure S1. SEM images of (a) carbon paper and (b) NiFe-GA-CP.

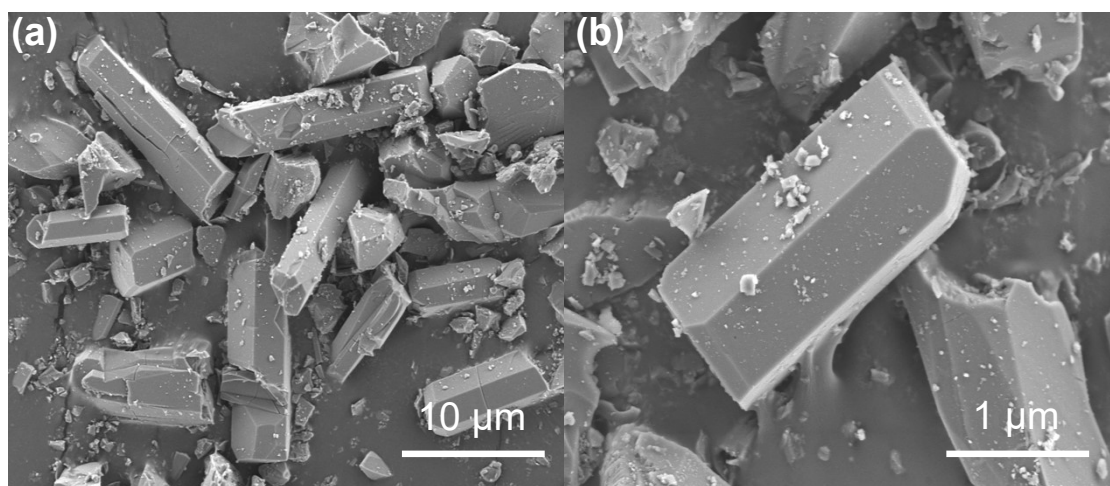


Figure S2. SEM images of NiFe-GA powder at different magnifications.

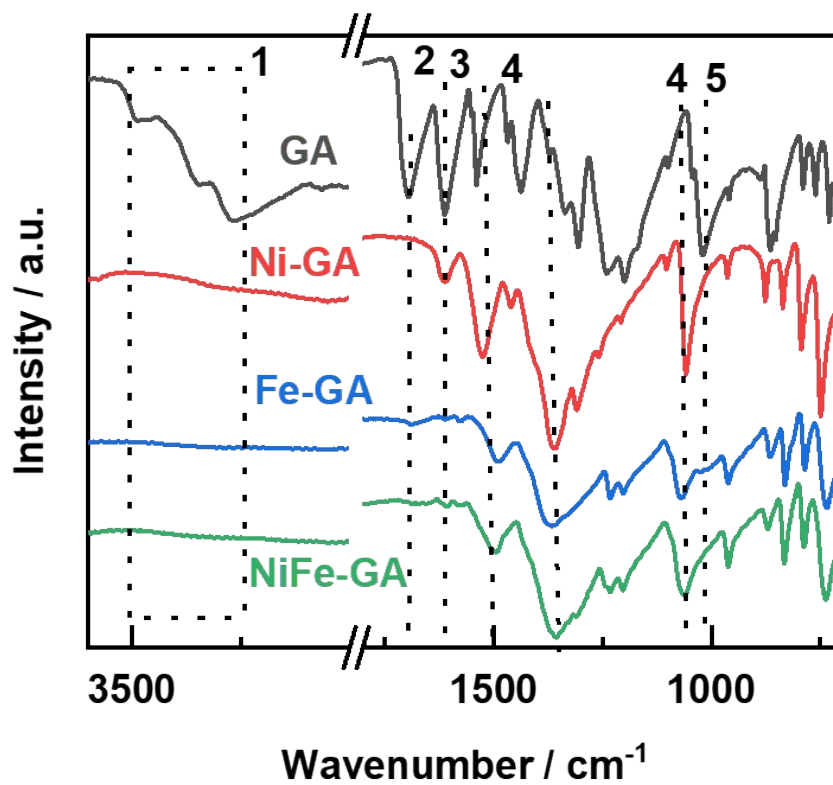


Figure S3. IR spectra of Ni-GA (red), Fe-GA (blue), NiFe-GA (green) and GA (black). The band assignments are listed in **Table S2**.

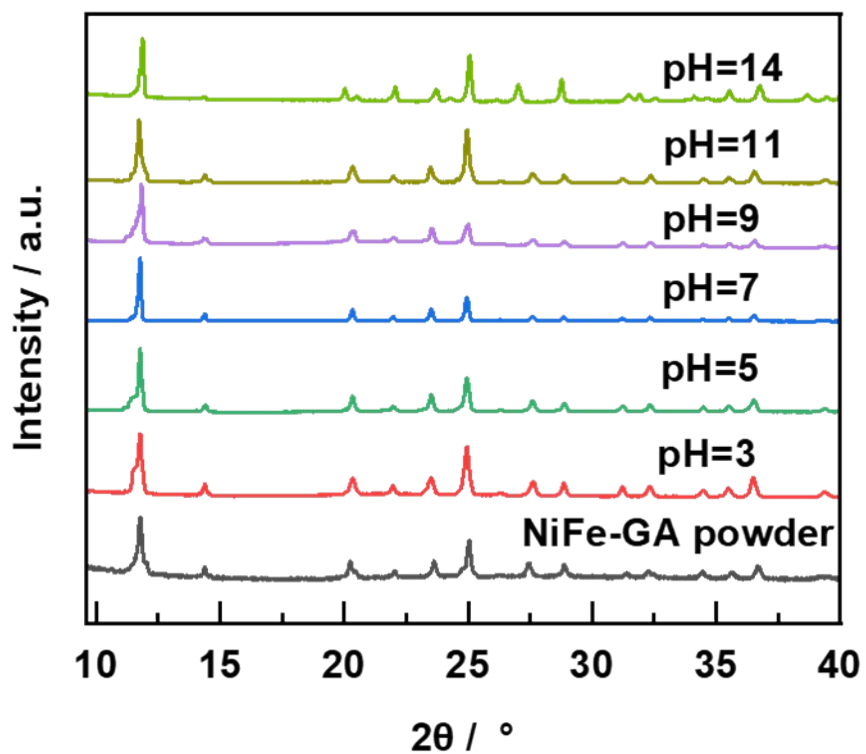


Figure S4. XRD patterns of NiFe-GA, with the as-synthesized catalyst immersed in aqueous solution of different pH values at room temperature for 24 h (HCl solution for pH=3/5, deionized water for pH=7, KOH solution for pH=9/11/14).

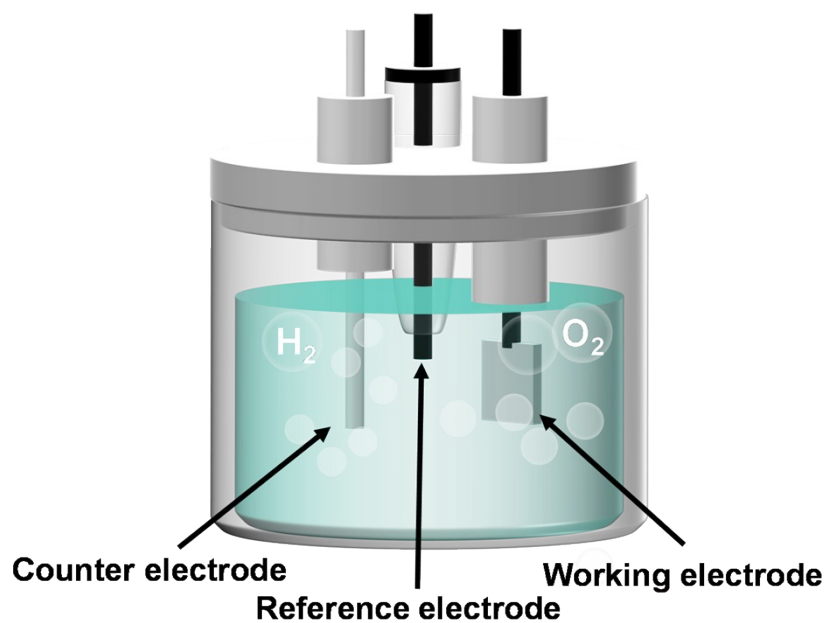


Figure S5. A standard three-electrode electrochemical cell: working electrode (modified CP); reference electrode (Hg/HgO); counter electrode (platinum wire).

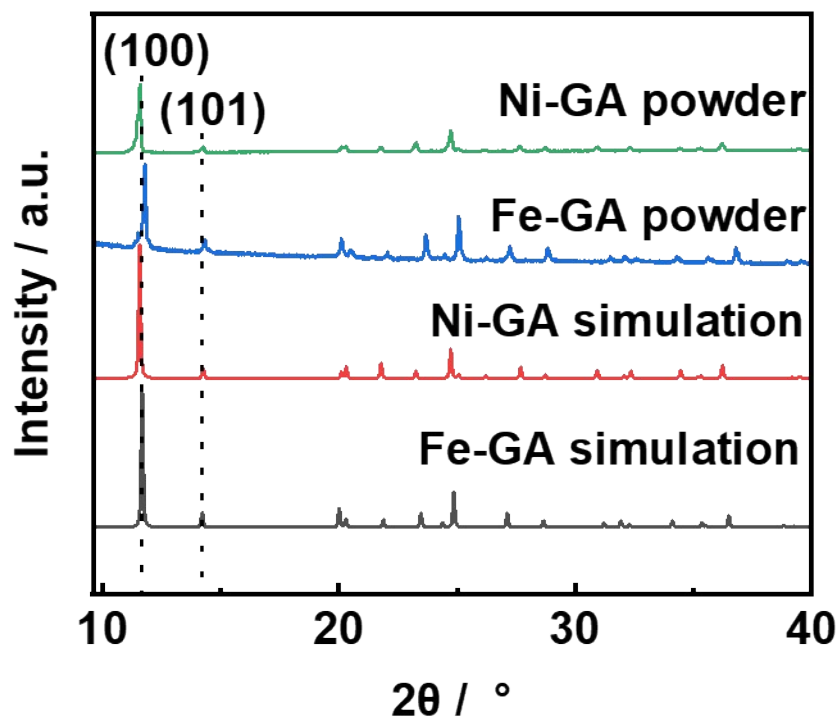


Figure S6. PXRD patterns of Fe-GA (blue) and Ni-GA (green). Simulated PXRD patterns of Fe-GA (black) and Ni-GA (red).

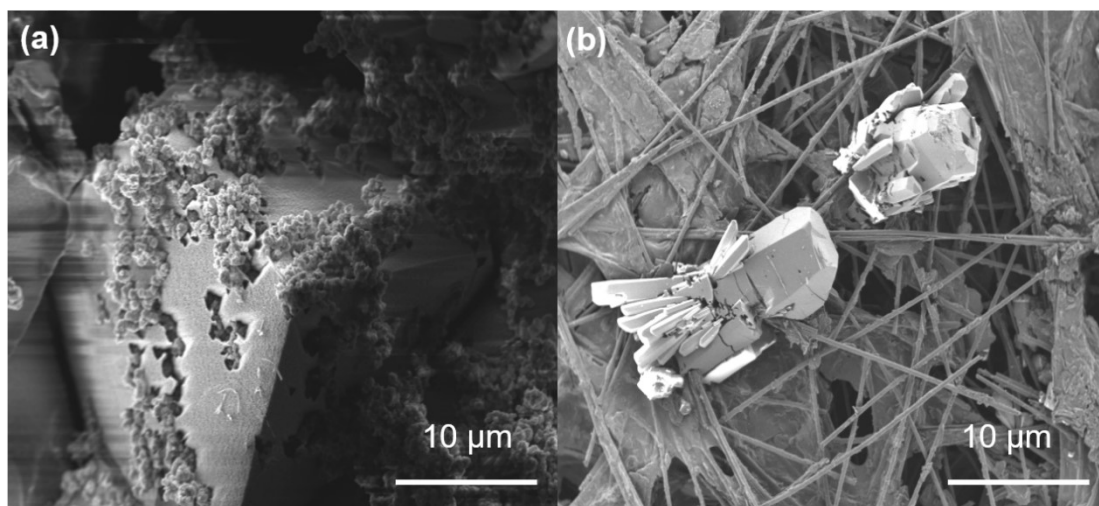


Figure S7. SEM images of (a) Ni-GA-CP and (b) Fe-GA-CP.

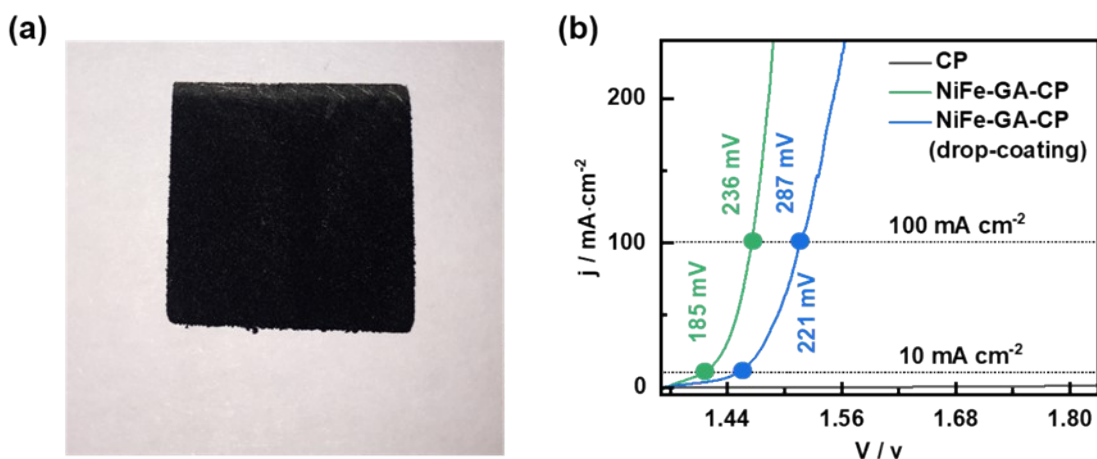


Figure S8. (a) As-prepared electrode by one-pot hydrothermal method; (b) LSV curves of the CP, NiFe-GA-CP and NiFe-GA-CP (drop-coating) in 1 M KOH. Potentials are reported versus RHE (RHE = reversible hydrogen electrode).

The NiFe-GA-CP (drop-coating) was prepared by drop-coating the ink containing Nafion solution and powder NiFe-GA ($\sim 11 \text{ mg}\cdot\text{cm}^{-2}$) on carbon paper. The NiFe-GA-CP (drop-coating) gives to the overpotentials of 221 mV at $j = 10 \text{ mA}\cdot\text{cm}^{-2}$ and 287 mV at $j = 100 \text{ mA}\cdot\text{cm}^{-2}$, which is worse than the OER performance of NiFe-GA-CP (solvothermal) with the overpotentials of 185 and 236 mV at the current densities of 10 and $100 \text{ mA}\cdot\text{cm}^{-2}$, respectively. We attributed the superior OER performance of NiFe-GA-CP (solvothermal) to the strong coupling effect between the catalytic material and the substrate.

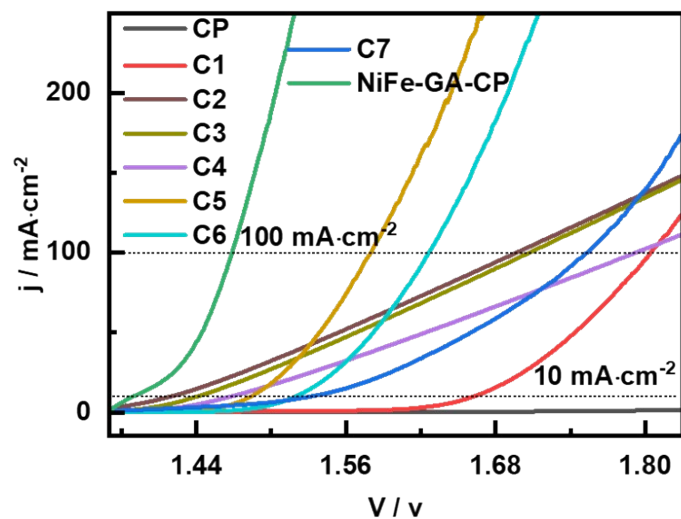


Figure S9. LSV curves of the CP, NiFe-GA-CP and the other reference samples of $\text{Ni}_x\text{Fe}_{2-x}\text{-GA-CP}$ (C1: Fe-GA-CP; C2: $\text{Ni}_{1.5}\text{Fe}_{0.5}\text{-GA-CP}$; C3: $\text{Ni}_{1.25}\text{Fe}_{0.75}\text{-GA-CP}$; C4: $\text{Ni}_1\text{Fe}_1\text{-GA-CP}$; C5: $\text{Ni}_{0.5}\text{Fe}_{1.5}\text{-GA-CP}$; C6: $\text{Ni}_{0.25}\text{Fe}_{1.75}\text{-GA-CP}$; C7: Ni-GA-CP) in 1 M KOH. Potentials are reported versus RHE (RHE = reversible hydrogen electrode).

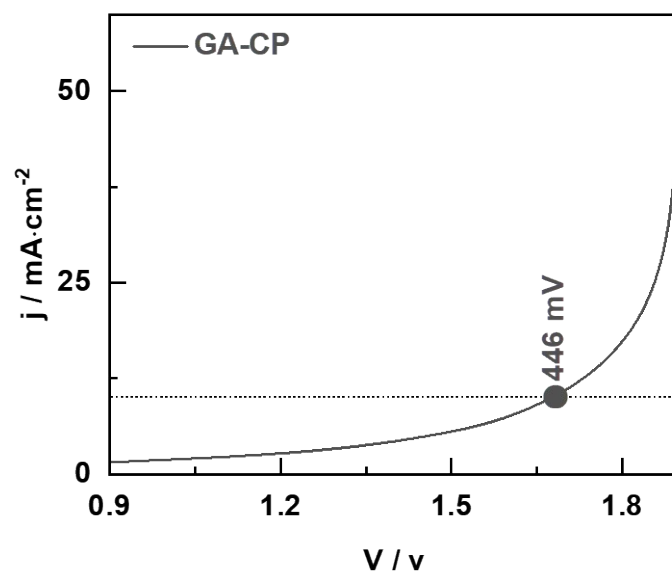


Figure S10 LSV curve of the GA-CP, in 1 M KOH. Potentials are reported versus RHE (RHE = reversible hydrogen electrode).

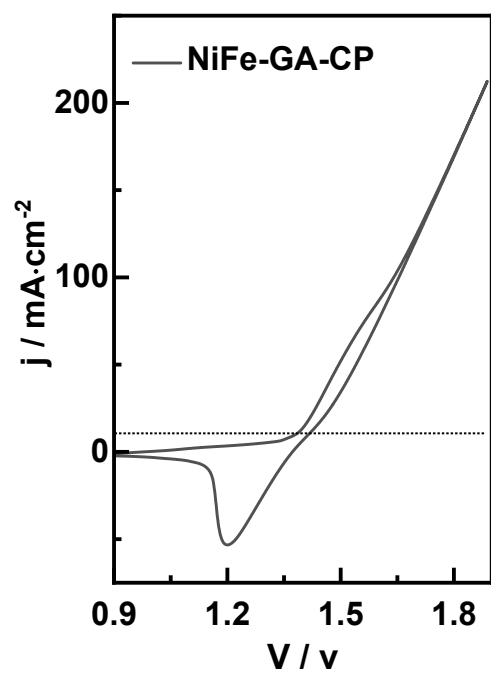


Figure S11. Cyclic voltammogram of NiFe-GA-CP in 1 M KOH at a scan rate of $5 \text{ mV}\cdot\text{s}^{-1}$.

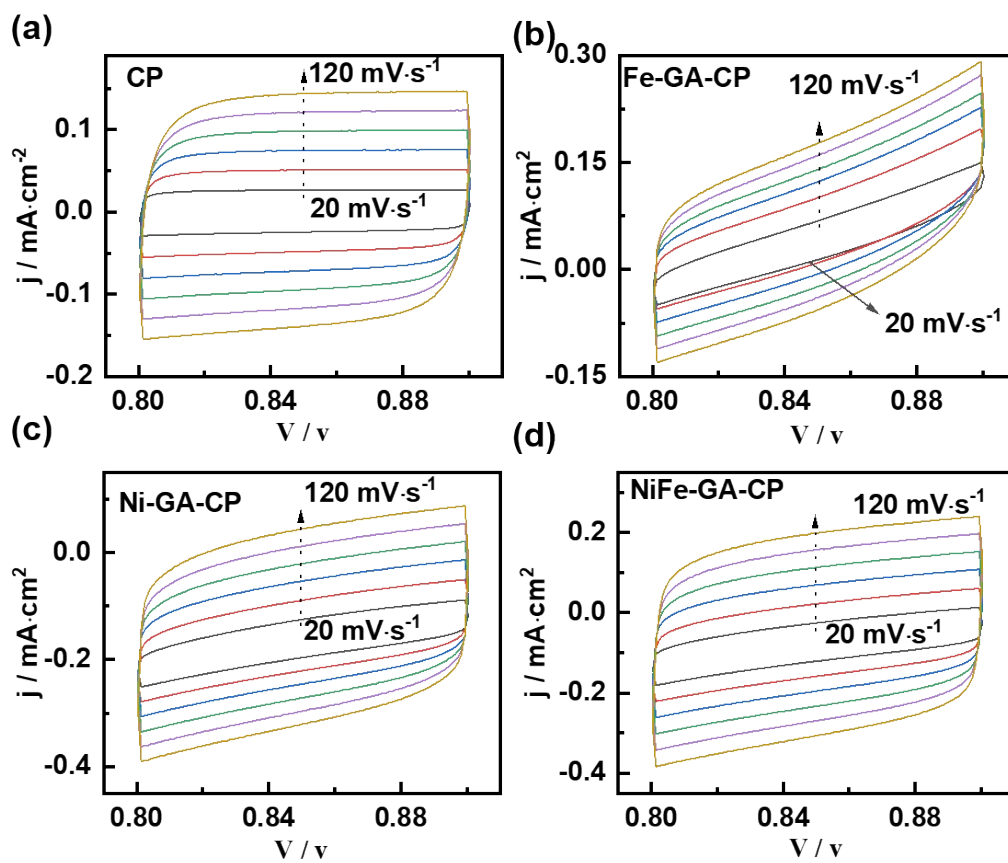


Figure S12. CV curves of (a) CP, (b) Fe-GA-CP, (c) Ni-GA-CP, and (d) NiFe-GA-CP (with varying scan rates: 20, 40, 60, 80, 100 and 120 $\text{mV}\cdot\text{s}^{-1}$) in 1 M KOH.

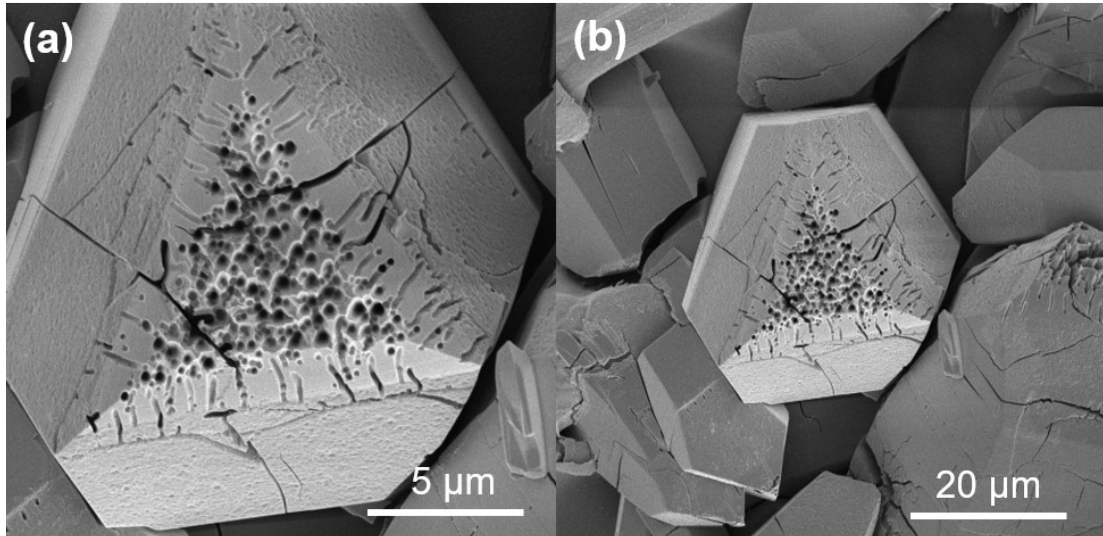


Figure S13. SEM images of NiFe-GA-CP after OER test at different magnifications.

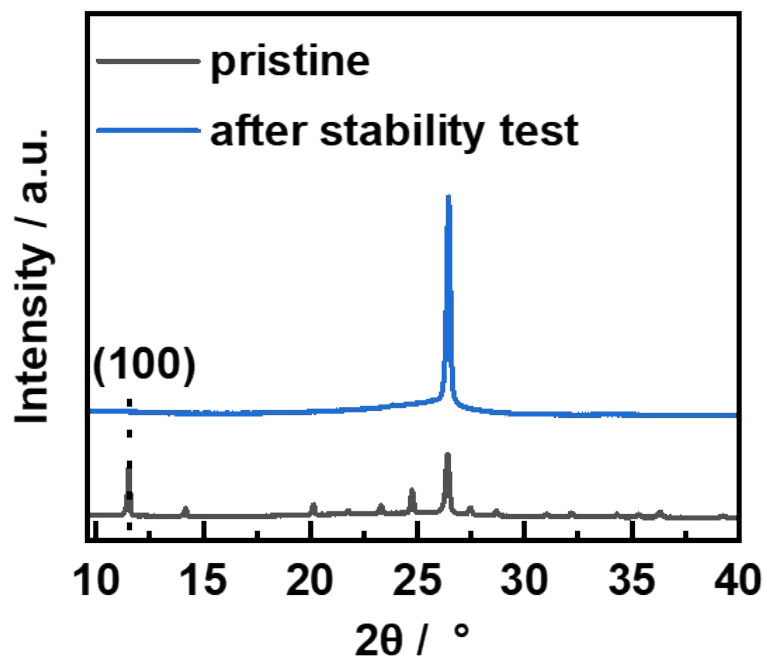


Figure S14. XRD pattern of NiFe-GA-CP before (black) and after (blue) stability test.

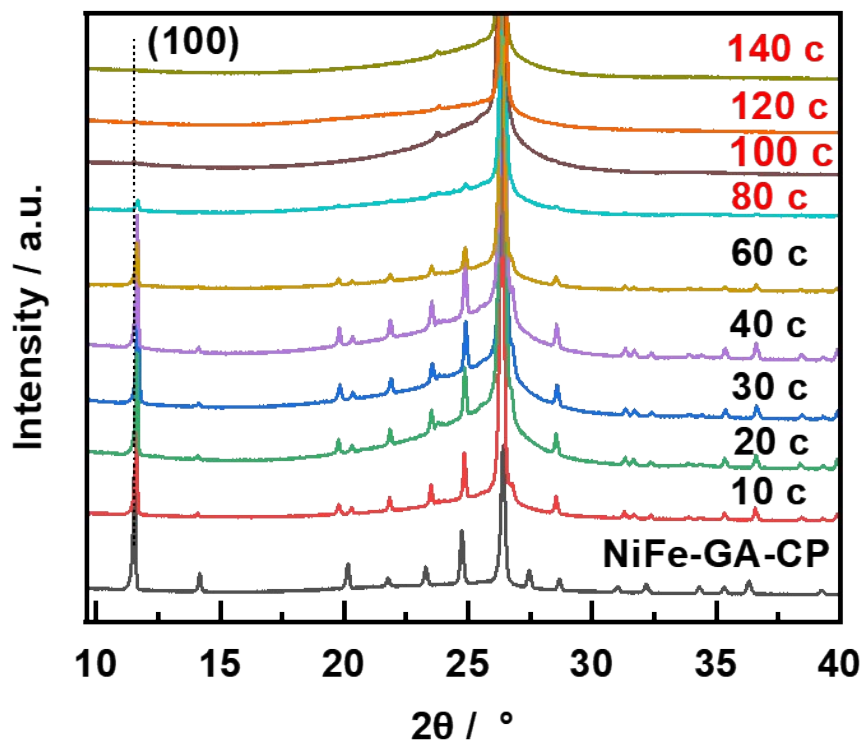


Figure S15. XRD patterns of NiFe-GA-CP and after different CV cycles in 1M KOH solution (CV: the range of 0.9 - 1.9 V vs. RHE at a scan rate of 50 mV s⁻¹).

In order to confirm whether OER performance originates from pristine NiFe-GA-CP or the reconstructed material, we have characterized the XRD patterns of NiFe-GA-CP with various CV cycles as show in **Figure S5**. Within 60 CV cycles, the crystalline structure of NiFe-GA-CP is remained, and the intensity of the (100) peak has a significant drop at 80 CV cycles, implying the occurrence of reconstruction of NiFe-GA-CP. This peak completely vanished when the CV cycles up to 140, indicating the transformation of NiFe-GA-CP into an amorphous ultrathin two-dimensional oxyhydroxide.

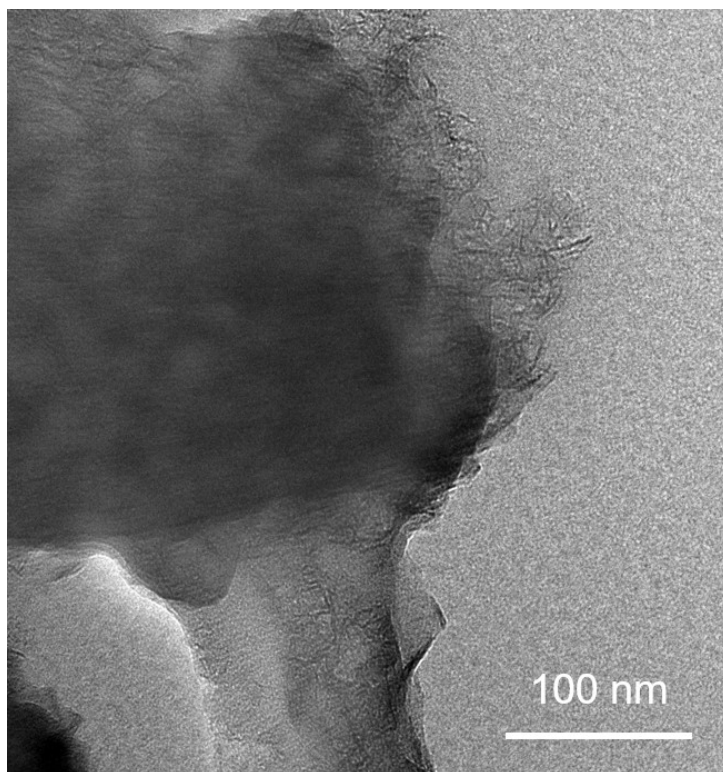


Figure S16. TEM image of NiFe-GA-CP after stability test.

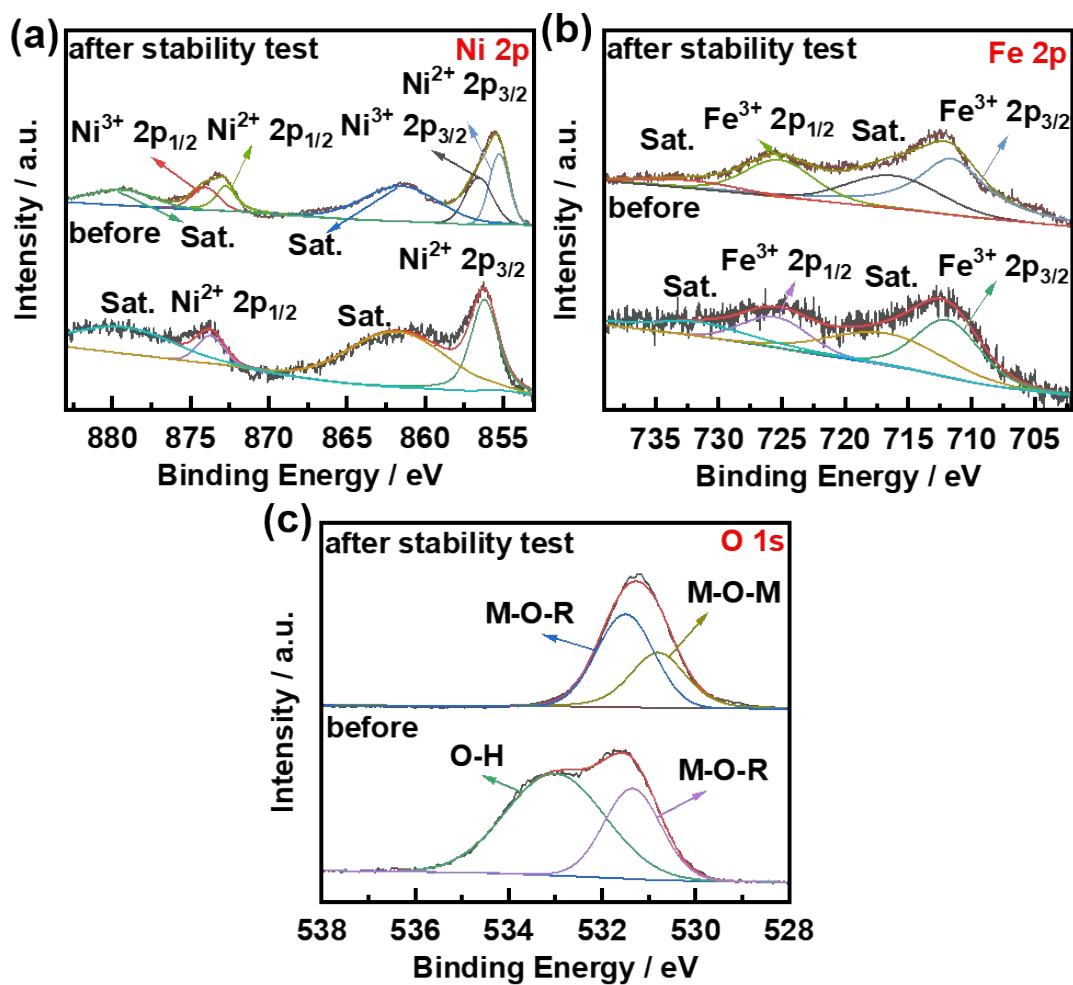


Figure S17. XPS spectra of NiFe-GA-CP before and after durability tests. (a) Ni 2p region; (b) Fe 2p region; and (c) O 1s region.

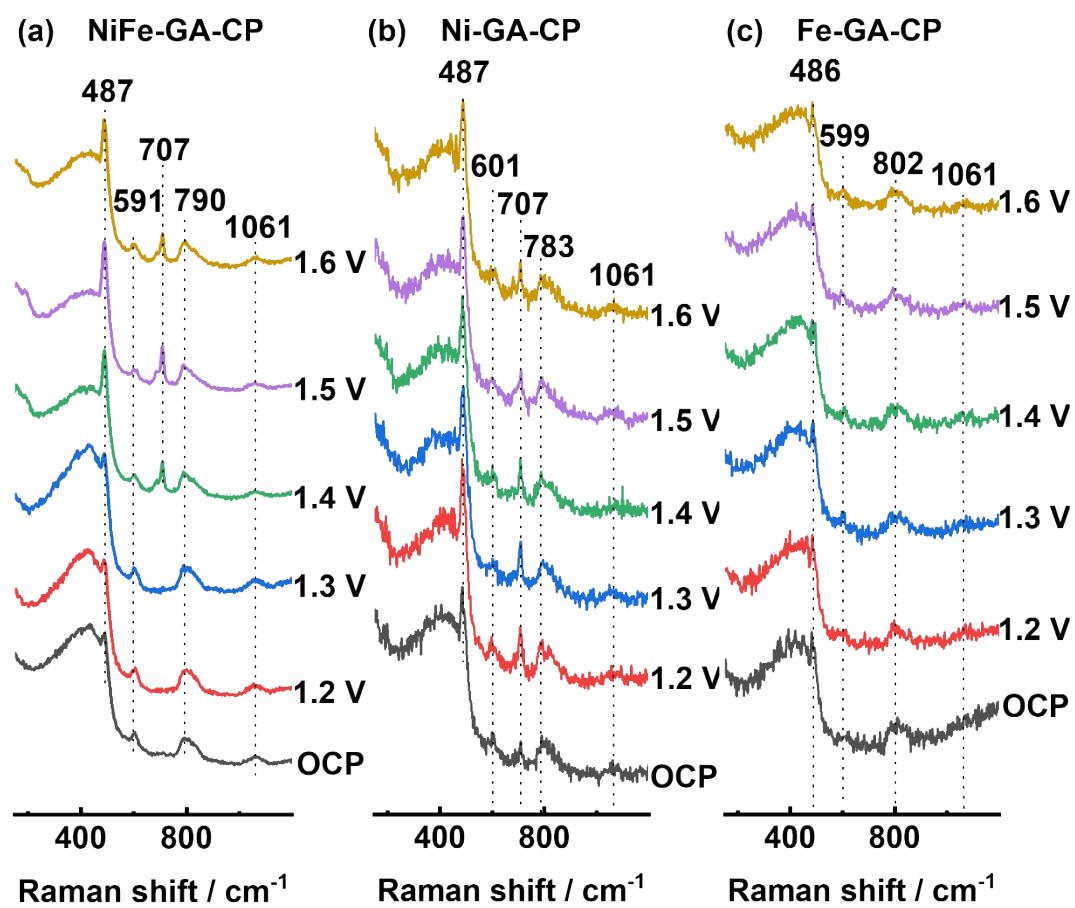


Figure S18. In-situ Raman spectra of (a) NiFe-GA-CP; (b) Ni-GA-CP; (c) Fe-GA-CP recorded at varied potentials during OER in 1 M KOH. OCP: open circuit potential.

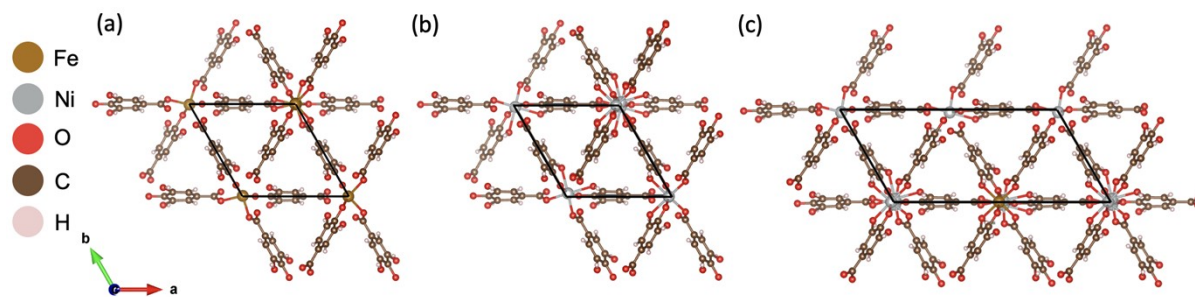


Figure S19. DFT optimized bulk structure of (a) Fe-GA (with lattice parameters of ($a = 9.1 \text{ \AA}$, $b = 9.1 \text{ \AA}$, $c = 9.9 \text{ \AA}$, $\alpha = 90^\circ$, $\beta = 90^\circ$, $\gamma = 120^\circ$)); (b) Ni-GA (with lattice parameters of ($a = 8.8 \text{ \AA}$, $b = 8.8 \text{ \AA}$, $c = 10.2 \text{ \AA}$, $\alpha = 89^\circ$, $\beta = 90^\circ$, $\gamma = 120^\circ$)); and NiFe-GA (with lattice parameters of ($a = 17.8 \text{ \AA}$, $b = 8.8 \text{ \AA}$, $c = 10.2 \text{ \AA}$, $\alpha = 89^\circ$, $\beta = 90^\circ$, $\gamma = 120^\circ$)).

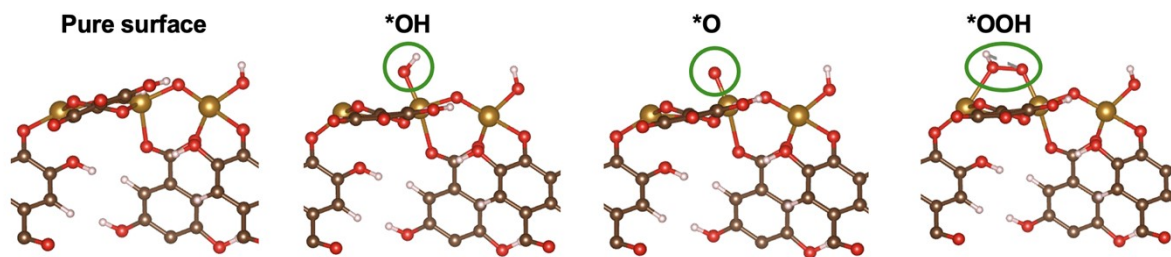


Figure S20. Optimized adsorption configurations of OER intermediates on the (100) surface of Fe-GA.

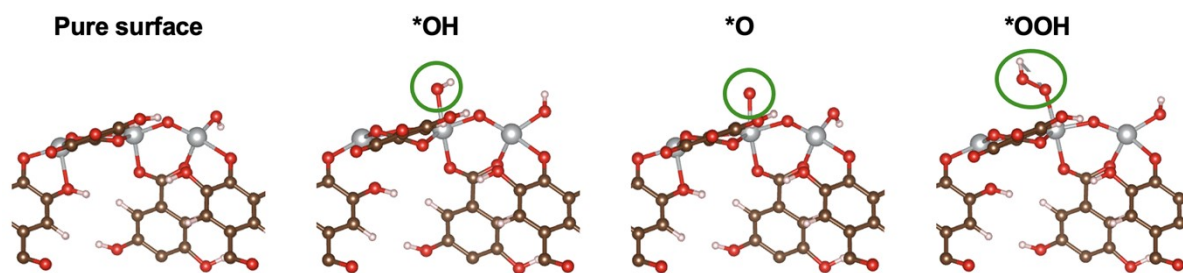


Figure S21. Optimized adsorption configurations of OER intermediates on the (100) surface of Ni-GA.

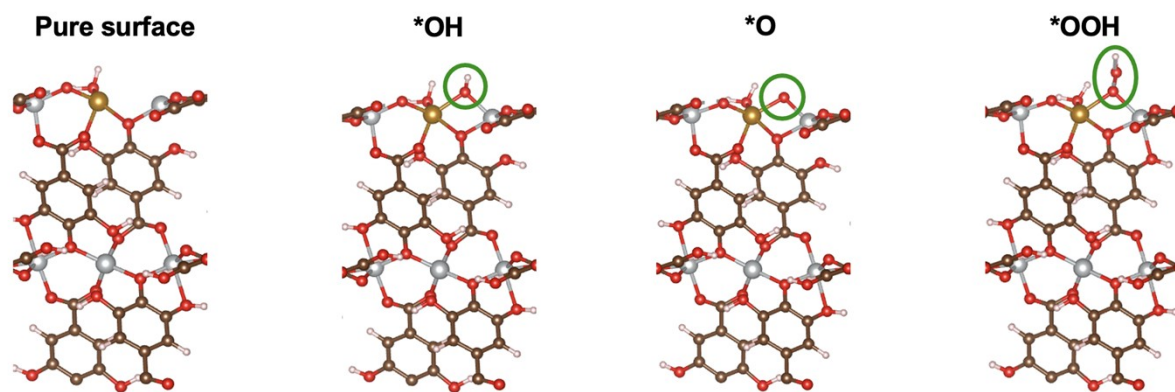


Figure S22. Optimized adsorption configurations of OER intermediates on the (100) surface of NiFe-GA.

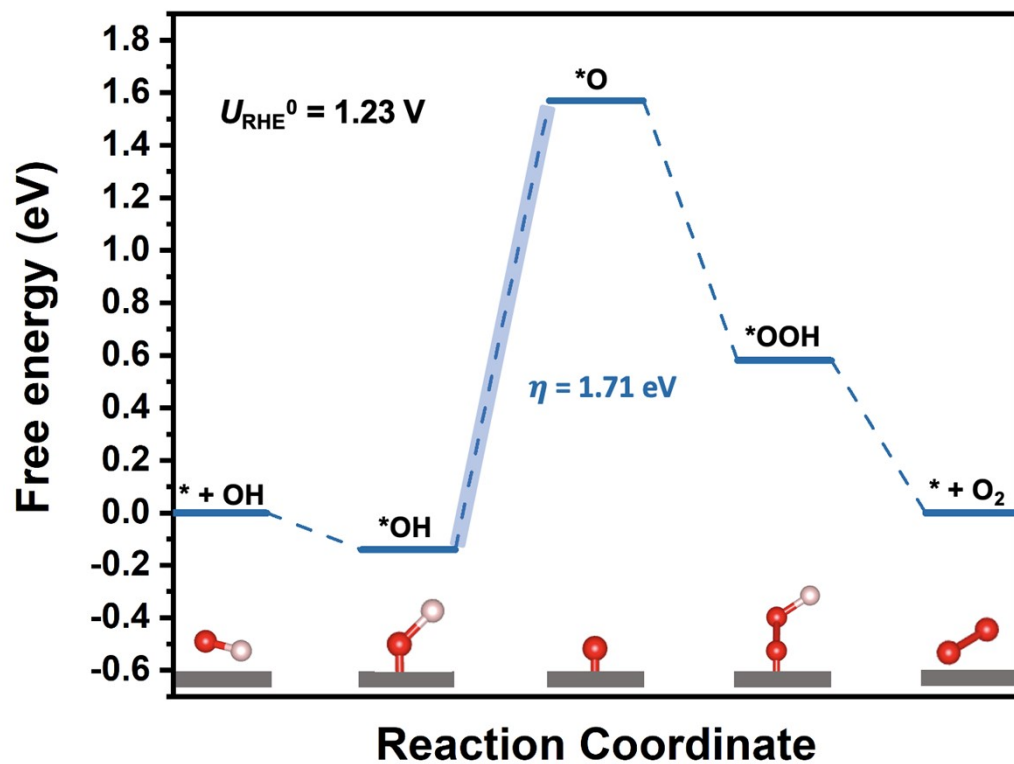


Figure S23. Calculated free energy diagram of the OER process on Fe-GA.

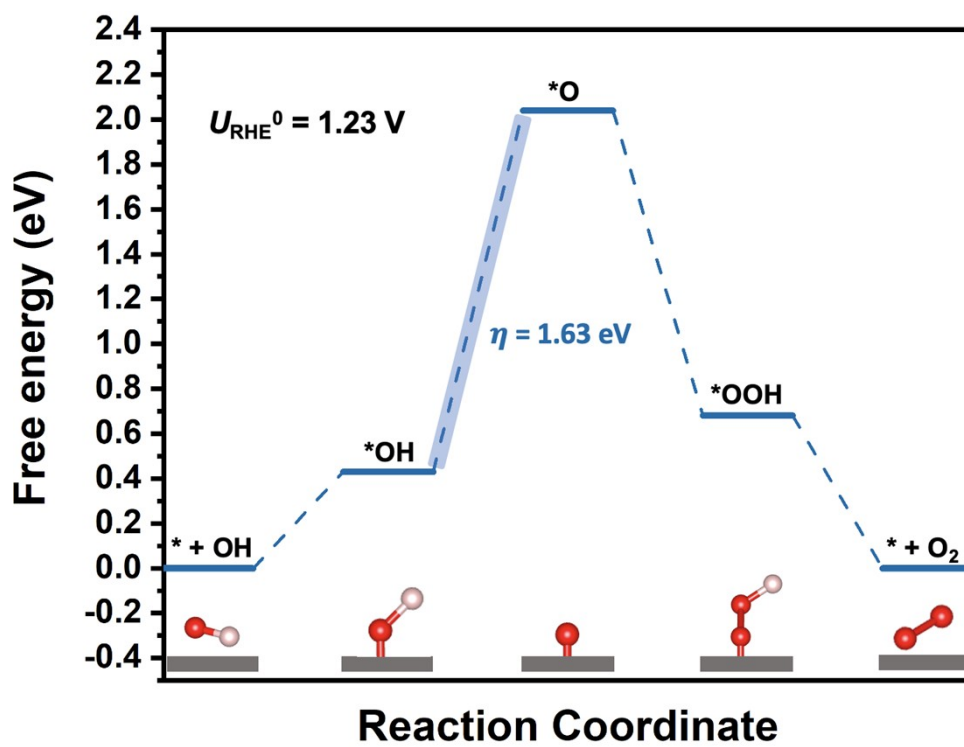


Figure S24. Calculated free energy diagram of the OER process on Ni-GA.

Table S1. EDS and ICP results of NiFe-GA MOF.

	Element	Weight %	Atom %	Concentration / mg·L⁻¹	Ni : Fe
EDS	Fe	4.58	1.35		~ 3:1
	Ni	13.08	3.67		
ICP	Fe			11.71	~ 3:1
	Ni			28.89	

Table S2. IR band assignments of Ni-GA, Fe-GA, NiFe-GA and GA.¹¹

	Wavenumber / cm⁻¹	Assignment	Group
1	3500~3200	ν O-H	-OH
2	1695	ν C=O	-COOH
3	1614	ν C=O	-CO-
4	1503	ν_{as} C=O	-COO-
5	1360	ν_s C=O	-COO-
6	1063	ν C-O	R-O-
7	1017	ν C-O	R-OH

Table S3. Catalyst concentrations of NiFe-GA, Fe-GA, and Ni-GA on CP.

Catalyst	Concentration / mg·cm⁻²
NiFe-GA-CP	11.44
Fe-GA-CP	11.25
Ni-GA-CP	11.30

Table S4. Comparison of the OER performance among NiFe-GA-CP and other electrocatalysts on carbon paper.

Catalyst	Substrate	j (mA·cm ⁻²)	η (mV)	Tafel slope (mV·dec ⁻¹)	Ref.
NiFe-GA-CP	CP	10	185	28.74	This Work
Ni-BTC	CP	10	346	64	12
Ni _{0.55} Fe _{0.45} -poly(5Aphen)/CP	CP	10	264		13
NiS@N/S-C	CP	10	417	48	14
CNH-D-NiMOF	CP	10	320	85.3	15
Ni-doped CoS ₂ /CFP	CFP	10	270	79	16
Zn-doped CoSe ₂	CP	10	356	88	17
NiFe NCs	CP	10	270	48	18
NiFe _x /NiFe ₂ O ₄ @NC	CP	10	262	51.4	19
Ni-Cu@Cu-Ni MOF	CP	10	624	98	20
(Fe _{0.5} Ni _{0.5})S ₂	CP	10	241	51.8	21
CNH-D-NiMOF-400	CP	20	270	97.2	15
		100	340		
Ni-Co-S/CF	CP	100	360	109	22
NiCo-LDH@FeOOH/CFP	CFP	10	224	38	23
NiFeCH(Ce)	CP	100	252	59	24
Co ₂ Fe _{0.5} V _{0.5} LDH	CP	10	242	41.4	25
NC/Co/CoP/CP	CP	10	350	94	26
N-CoSe ₂ @CP	CP	10	273	74	27
Co(OH) _x /Ag/Co(OH) ₂	CP	10	283	97	28
CuCo-MOF	CP	10	340	173.5	29
Ni-Cu@Cu-Ni-MOF	CP	10	624	98	20
GNiPy350N	CP	10	320	52.2	30
NiCoP-CNT@NiCo/CP	CP	10	290	21	31
NiCoFeP/C	CP	10	270	87	32
Fe-Co-P	CP	10	269	31	33
Cu _{0.075} Co _{0.925} P/CP	CP	10	221	70.4	34
Co _x Fe _y N/graphene	CP	10	270	32	35
MCCF/NiMn-MOF	CP	10	280	86	36

Table S5. Comparison of the OER performance among NiFe-GA-CP and other electrocatalysts on nickel foam (NF) at 10 mA·cm⁻².

Catalyst	Substrate	j (mA·cm ⁻²)	η (mV)	Tafel slope (mV·dec ⁻¹)	Ref.
NiFe-GA-CP	CP	10	185	28.74	This Work
Mn-doped NiFe-LDH	NF	10	250	47	37
CoFe LDHs-Ar	NF	10	266	37.85	38
NiFe-LDH	NF	10	210	40.4	39
NiFeRu-LDH	NF	10	225	31	40
NiFeMo	NF	10	280	40	41
Ni _{0.7} Fe _{0.3} S ₂	NF	10	198	56	42
Ni _{0.65} Ga _{0.30} Fe _{0.05} /NF	NF	10	200	42	43
NF-Na-Fe-Pt	NF	10	261	39.68	44
a/c-NiFe-G	NF	10	250	36.5	45
Ni _{1/2} Fe _{1/2} (OH) ₂ /CNT	NF	10	244	41	46
NiCoFe-PS nanorod/NF	NF	10	195	40.3	47
P-Ni _{0.75} Fe _{0.25} Se ₂	NF	10	156	19.5	48
CoMoNiS-NF-31	NF	10	166	58	49
Ni-Fe-Se nanocages	NF	10	249	36	50
NiFe-polydopamine film	NF	10	254.1	23.3	51
MCCF/NiMn-MOF	NF	10	195	44.1	52

Table S6. Comparison of the OER performance among NiFe-GA-CP and other electrocatalysts at 100 mA cm⁻².

Catalyst	j (mA·cm ⁻²)	η (mV)	Stability (h)	Tafel slope (mV·dec ⁻¹)	Ref.
NiFe-GA-CP	100	236	24	28.74	This Work
S-(Ni,Fe)OOH	100	281	100	48.9	53
Ta-NiFe LDH	100	280	20	58.95	54
NiMoFeO@NC	100	290	24	66.6	55
Ni _{0.75} Fe _{0.25} Se ₂ by P doping	100	238	120	27.2	56
Ru ₁ /D-NiFe LDH	100	218	100	31	57
Ni(OH) ₂ /FeOOH	100	247	110	27.7	58
(WO ₂ -Na _x WO ₃)@FeOOH/NF	100	260	120	42.2	59
Ni(Fe)OOH-FeS _x	100	310	16	55	60
FeNi(VO ₄) _x @NF	100	274	11	56.6	61
FeOOH/Co/FeOOH HNTAs-NF	100	300	50	32	62
Au/NiFe-LDH	100	240	20	40.4	63
Cu@NiFe LDH	100	281	48	27.8	64
Ni ₃ Fe _{0.5} V _{0.5}	100	264	60	39	65
NiMoFeO@NC	100	290	24	66.6	66

Table S7. XPS fitting results of NiFe-GA-CP before and after stability test.

		BE / eV	BE /eV	Valence
		2p _{3/2}	2p _{1/2}	
Ni 2p	Before	856.2	873.7	
	After	854.8	872.2	+2
	stability test	855.8	873.2	+3
Fe 2p	Before	711.9	725.5	
	After	711.5	724.4	+3
	stability test			
				Assignment
O 1s	Before	531.4		M-O-R
		533.0		chemisorbed molecular water
	After	530.8		M-O-M
	stability test	531.5		M-O-R

Table S8. Raman band assignments of NiFe-GA-CP, Ni-GA-CP, and Fe-GA-CP.

	Raman shift / cm ⁻¹	Assignment	Ref.
NiFe-GA-CP	487	NiOOH / Fe-O	67, 68
	591	FeOOH	69
	707	FeOOH / NiO	70, 71
	790	Ni-H	72
	1061	active oxygen / Ni-O	71, 73
Ni-GA-CP	487	NiOOH	67
	601	Ni(OH) ₂	71
	707	NiO	71
	783	Ni-H	72
	1061	Ni-O	71
Fe-GA-CP	486	Fe-O	68
	599	FeOOH	69
	802	C-H	74
	1061	active oxygen	73

Table S9. DFT calculated free energy changes of each step in the OER process on Fe-GA, Ni-GA, and NiFe-GA.

OER Descriptors	Fe-GA	Ni-GA	NiFe-GA
ΔG^*	0 eV	0 eV	0 eV
ΔG^*_{OH}	-0.14 eV	0.43 eV	-0.33 eV
ΔG^*_{O}	1.57 eV	2.06 eV	-0.06 eV
ΔG^*_{OOH}	0.58 eV	0.68 eV	0.03 eV
Overpotential	1.71 eV	1.63 eV	0.27 eV

References

1. J. Zhu, F. Chen, Z. Zhang, M. Li, Q. Yang, Y. Yang, Z. Bao and Q. Ren, *ACS Sustain. Chem. Eng.*, 2019, **7**, 12955-12963.
2. J. Wang, L. Li, L. Guo, Y. Zhao, D. Xie, Z. Zhang, Q. Yang, Y. Yang, Z. Bao and Q. Ren, *Chemistry*, 2019, **25**, 15516-15524.
3. R. K. Feller and A. K. Cheetham, *Solid State Sci.*, 2006, **8**, 1121-1125.
4. G. Kresse and J. Furthmüller, *Phys. Rev. B - Condens. Matter Mater. Phys.*, 1996, **54 (16)**, 11169–11186.
5. P. E. Blochl, *Rev. B - Condens. Matter Mater. Phys.*, 1994, **50**, 17953-17979.
6. D. Joubert, *Phys. Rev. B - Condens. Matter Mater. Phys.*, 1999, **59 (3)**, 1758–1775.
7. J. P. Perdew, K. Burke and M. Ernzerhof, *Phys. Rev. Lett.*, 1996, **77 (18)**, 3865–3868.
8. S. Grimme, J. Antony, S. Ehrlich and H. Krieg, *J. Chem. Phys.*, 2010, **132**, 154104.
9. S. Zhao, Y. Wang, J. Dong, C.-T. He, H. Yin, P. An, K. Zhao, X. Zhang, C. Gao, L. Zhang, J. Lv, J. Wang, J. Zhang, A. M. Khattak, N. A. Khan, Z. Wei, J. Zhang, S. Liu, H. Zhao and Z. Tang, *Nat. Energy.*, 2016, **1**, 16184.
10. J. K. Nørskov, J. Rossmeisl, A. Logadottir, L. Lindqvist, J. R. Kitchin, T. Bligaard and H. Jónsson, *J. Phys. Chem. B*, 2004, **108 (46)**, 17886–17892.
11. A. Sharma, A. Kumar, C. Li, P. Panwar Hazari, S. D. Mahajan, R. Aalinkeel, R. K. Sharma and M. T. Swihart, *J. Mater. Chem. B*, 2021, **9**, 2505-2514.
12. V. Maruthapandian, S. Kumaraguru, S. Mohan, V. Saraswathy and S. Muralidharan, *ChemElectroChem*, 2018, **5**, 2795-2807.
13. Z. Zhou, Q. Tian, L. Chai, P. Chao, S. Liu and C. Wang, *J. Power Sources*, 2021, **506**, 230109.
14. L. Yang, M. Gao, B. Dai, X. Guo, Z. Liu and B. Peng, *Electrochim. Acta*, 2016, **191**, 813-820.
15. Y. Guo, Y. Zhou, Y. Nan, B. Li and X. Song, *ACS Appl. Mater. Interfaces*, 2020, **12**, 12743-12754.
16. Z. Xie, H. Tang and Y. Wang, *ChemElectroChem*, 2019, **6**, 1206-1212.
17. Q. Dong, Q. Wang, Z. Dai, H. Qiu and X. Dong, *ACS Appl. Mater. Interfaces*, 2016, **8**, 26902-26907.
18. A. Kumar and S. Bhattacharyya, *ACS Appl. Mater. Interfaces*, 2017, **9**, 41906-41915.
19. J. Zhao, X. Zhang, M. Liu, Y.-Z. Jiang, M. Wang, Z.-Y. Li and Z. Zhou, *J. Mater. Chem. A*, 2019, **7**, 21338-21348.
20. X. Ma, K. Qi, S. Wei, L. Zhang and X. Cui, *J. Alloys Compd.*, 2019, **770**, 236-242.
21. W. Dai, Y. Pan, K. Ren, Y.-a. Zhu and T. Lu, *Electrochim. Acta*, 2020, **355**, 136821.
22. T. Liu, X. Sun, A. M. Asiri and Y. He, *Int. J. Hydrog. Energy*, 2016, **41**, 7264-7269.

23. X. Han, Y. Niu, C. Yu, Z. Liu, H. Huang, H. Huang, S. Li, W. Guo, X. Tan and J. Qiu, *Nano Energy*, 2020, **69**, 104367.
24. J. Cai, J. Huang, S. Xu, L. Yuan, X. Huang, Z. Huang and C. Zhang, *J. Solid State Electro.*, 2019, **23**, 3449-3458.
25. Y. Yang, Y. Ou, Y. Yang, X. Wei, D. Gao, L. Yang, Y. Xiong, H. Dong, P. Xiao and Y. Zhang, *Nanoscale*, 2019, **11**, 23296-23303.
26. M. Cong, D. Sun, L. Zhang and X. Ding, *Chinese J. Catal.*, 2020, **41**, 242-248.
27. G. Wei, Z. Xu, X. Zhao, S. Wang, F. Kong and C. An, *J. Alloys Compd.*, 2022, **893**, 162328.
28. W. Guo, J. Kim, H. Kim, G. H. Han, H. W. Jang, S. Y. Kim and S. H. Ahn, *J. Alloys Compd.*, 2022, **889**, 161674.
29. Q. Liu, J. Chen, F. Yu, J. Wu, Z. Liu and B. Peng, *New. J. Chem.*, 2021, **45**, 16714-16721.
30. A. S. Souza, L. S. Bezerra, E. S. F. Cardoso, G. V. Fortunato and G. Maia, *J. Mater. Chem. A*, 2021, **9**, 11255-11267.
31. Z. Wang, C. Wei, X. Zhu, X. Wang, J. He and Y. Zhao, *J. Mater. Chem. A*, 2021, **9**, 1150-1158.
32. X. Wei, Y. Zhang, H. He, L. Peng, S. Xiao, S. Yao and P. Xiao, *Chem. Commun.*, 2019, **55**, 10896-10899.
33. H. Zhang, W. Zhou, J. Dong, X. F. Lu and X. W. Lou, *Energy Environ. Sci.*, 2019, **12**, 3348-3355.
34. L. Yan, B. Zhang, J. Zhu, S. Zhao, Y. Li, B. Zhang, J. Jiang, X. Ji, H. Zhang and P. K. Shen, *J. Mater. Chem. A*, 2019, **7**, 14271-14279.
35. H. Liu, X. Lu, Y. Hu, R. Chen, P. Zhao, L. Wang, G. Zhu, L. Ma and Z. Jin, *J. Mater. Chem. A*, 2019, **7**, 12489-12497.
36. W. Cheng, X. F. Lu, D. Luan and X. W. D. Lou, *Angew. Chem. Int. Ed.*, 2020, **59**, 18234-18239.
37. Z. Lu, L. Qian, Y. Tian, Y. Li, X. Sun and X. Duan, *Chem. Commun.*, 2016, **52**, 908-911.
38. Y. Wang, Y. Zhang, Z. Liu, C. Xie, S. Feng, D. Liu, M. Shao and S. Wang, *Angew. Chem. Int. Ed.*, 2017, **56**, 5867-5871.
39. X. Yang, C.-J. Wang, C.-C. Hou, W.-F. Fu and Y. Chen, *ACS Sustain. Chem. Eng.*, 2018, **6**, 2893-2897.
40. G. Chen, T. Wang, J. Zhang, P. Liu, H. Sun, X. Zhuang, M. Chen and X. Feng, *Adv. Mater.*, 2018, **30**, 1706279.
41. N. Han, F. Zhao and Y. Li, *J. Mater. Chem. A*, 2015, **3**, 16348-16353.
42. J. Yu, G. Cheng and W. Luo, *J. Mater. Chem. A*, 2017, **5**, 15838-15844.
43. S. F. Zai, A. Q. Dong, J. Li, Z. Wen, C. C. Yang and Q. Jiang, *J. Mater. Chem. A*, 2021, **9**, 6223-6231.
44. Y. Zhao, Y. Gao, Z. Chen, Z. Li, T. Ma, Z. Wu and L. Wang, *Appl. Catal. B*, 2021, **297**, 120395.
45. Z. Gong, R. Liu, H. Gong, G. Ye, J. Liu, J. Dong, J. Liao, M. Yan, J. Liu, K. Huang, L. Xing, J. Liang, Y. He and H. Fei, *ACS Catal.*, 2021, **11**, 12284-12292.
46. J. Ge, J. Y. Zheng, J. Zhang, S. Jiang, L. Zhang, H. Wan, L. Wang, W. Ma, Z. Zhou and R. Ma, *J. Mater. Chem. A*, 2021, **9**, 14432-14443.
47. M. Yao, H. Hu, B. Sun, N. Wang, W. Hu and S. Komarneni, *Small*, 2019, **15**, 1905201.

48. Y. Huang, L.-W. Jiang, X.-L. Liu, T. Tan, H. Liu and J.-J. Wang, *Appl. Catal. B*, 2021, **299**, 120678.
49. Y. Yang, H. Yao, Z. Yu, S. M. Islam, H. He, M. Yuan, Y. Yue, K. Xu, W. Hao, G. Sun, H. Li, S. Ma, P. Zapol and M. G. Kanatzidis, *J. Am. Chem. Soc.*, 2019, **141**, 10417-10430.
50. Z. P. Wu, H. Zhang, S. Zuo, Y. Wang, S. L. Zhang, J. Zhang, S. Q. Zang and X. W. D. Lou, *Adv. Mater.*, 2021, **33**, 2103004.
51. L. Zhang, W. Tang, C. Dong, D. Zhou, X. Xing, W. Dong, Y. Ding, G. Wang and M. Wu, *Appl. Catal. B*, 2021, 120833.
52. J. Liang, X. Gao, B. Guo, Y. Ding, J. Yan, Z. Guo, E. C. M. Tse and J. Liu, *Angew. Chem. Int. Ed.*, 2021, **60**, 12770-12774.
53. L. Yu, L. Wu, B. McElhenny, S. Song, D. Luo, F. Zhang, Y. Yu, S. Chen and Z. Ren, *Energy Environ. Sci.*, 2020, **13**, 3439-3446.
54. X. Wang, Y. Tuo, Y. Zhou, D. Wang, S. Wang and J. Zhang, *Chem. Eng. J.*, 2021, **403**, 126297.
55. Y. Wang, Y. Zhu, S. Zhao, S. She, F. Zhang, Y. Chen, T. Williams, T. Gengenbach, L. Zu, H. Mao, W. Zhou, Z. Shao, H. Wang, J. Tang, D. Zhao and C. Selomulya, *Matter*, 2020, **3**, 2124-2137.
56. Y. Huang, L. W. Jiang, B. Y. Shi, K. M. Ryan and J. J. Wang, *Adv. Sci.*, 2021, 2101775.
57. P. Zhai, M. Xia, Y. Wu, G. Zhang, J. Gao, B. Zhang, S. Cao, Y. Zhang, Z. Li, Z. Fan, C. Wang, X. Zhang, J. T. Miller, L. Sun and J. Hou, *Nat. Commun.*, 2021, **12**, 4587.
58. H. Liao, T. Luo, P. Tan, K. Chen, L. Lu, Y. Liu, M. Liu and J. Pan, *Adv. Funct. Mater.*, 2021, 202102772.
59. J. Liu, G. Qian, H. Zhang, J. Chen, Y. Wang, H. He, L. Luo and S. Yin, *Chem. Eng. J.*, 2021, **426**, 131253.
60. H. Yang, L. Gong, H. Wang, C. Dong, J. Wang, K. Qi, H. Liu, X. Guo and B. Y. Xia, *Nat. Commun.*, 2020, **11**, 5075.
61. K. Dastafkan, Q. Meyer, X. Chen and C. Zhao, *Small*, 2020, **16**, 2002412.
62. J. X. Feng, H. Xu, Y. T. Dong, S. H. Ye, Y. X. Tong and G. R. Li, *Angew. Chem. Int. Ed.*, 2016, **55**, 3694-3698.
63. J. Zhang, J. Liu, L. Xi, Y. Yu, N. Chen, S. Sun, W. Wang, K. M. Lange and B. Zhang, *J. Am. Chem. Soc.*, 2018, **140**, 3876-3879.
64. L. Yu, H. Zhou, J. Sun, F. Qin, F. Yu, J. Bao, Y. Yu, S. Chen and Z. Ren, *Energy Environ. Sci.*, 2017, **10**, 1820-1827.
65. J. Jiang, F. Sun, S. Zhou, W. Hu, H. Zhang, J. Dong, Z. Jiang, J. Zhao, J. Li, W. Yan and M. Wang, *Nat. Commun.*, 2018, **9**, 2885.
66. Q. Che, Q. Li, X. Chen, Y. Tan and X. Xu, *Appl. Catal. B*, 2020, **263**, 118338.
67. D. Zhou, S. Wang, Y. Jia, X. Xiong, H. Yang, S. Liu, J. Tang, J. Zhang, D. Liu, L. Zheng, Y. Kuang, X. Sun and B. Liu, *Angew. Chem. Int. Ed.*, 2019, **58**, 736-740.
68. M. Legodi and D. Dewaal, *Dyes Pigm.*, 2007, **74**, 161-168.
69. K. Hedenstedt, J. Bäckström and E. Ahlberg, *J. Electrochem. Soc.*, 2017, **164**, 621-627.
70. L. Bai, S. Lee and X. Hu, *Angew. Chem. Int. Ed.*, 2021, **60**, 3095-3103.
71. W. Lai, L. Ge, H. Li, Y. Deng, B. Xu, B. Ouyang and E. Kan, *Int. J. Hydrog. Energy*, 2021, **46**, 26861-26872.

72. A. Y. Faid, A. O. Barnett, F. Seland and S. Sunde, *Electrochim. Acta*, 2020, **361**, 137040.
73. K. Wang, H. Du, S. He, L. Liu, K. Yang, J. Sun, Y. Liu, Z. Du, L. Xie, W. Ai and W. Huang, *Adv. Mater.*, 2021, **33**, 2005587.
74. K. C. Le, J. Henriksson and P. E. Bengtsson, *J Raman Spectrosc*, 2021, **52**, 1115-1122.